Characterisation of the Delphi Electronically Scanning Radar for Robotics Applications

Leo Stanislas
Polytech Paris-UPMC
University Paris 6, 75005, France

Thierry Peynot
Queensland University of Technology (QUT)
Brisbane QLD 4001, Australia

Abstract

Mm-wave radars have an important role to play in field robotics for applications that require reliable perception in challenging environmental conditions. This paper presents an experimental characterisation of the Delphi Electronically Scanning Radar (ESR) for mobile robotics applications. The performance of the sensor is evaluated in terms of detection ability and accuracy, for varying factors including: sensor temperature, time, target's position, speed, shape and material. We also evaluate the sensor's target separability performance.

1 Introduction

Mm-wave radars have an important role to play in field robotics for applications that require reliable perception in challenging environmental conditions, e.g. in the presence of fog, smoke or airborne dust [Peynot *et al.*, 2009; Gerardo-Castro and Peynot, 2012]. However, most high-performance mm-wave radars have remained too expensive to make them viable for use outside of mines. The Delphi Electronically Scanning Radar (ESR), shown in Fig. 1, has been designed for automotive applications and is aimed at mass production, which makes its cost more competitive. However, this is a fairly recent sensor, and little information about its field performance can be found in the literature, especially for robotics applications. This paper presents an experimental characterisation of the Delphi ESR for mobile robotics applications.

In [Fischer *et al.*, 2009], the ESR was used in a collision-avoidance system. It was evaluated in terms of vehicle detection reliability, position, speed and acceleration accuracy. The sensor was compared to a Smartmicro SMS UMRR9 radar and an Ibeo Lux laser scanner for the detection of cars coming to a highway intersection. The Delphi ESR was able to detect 99.995% of the cars as far as $180m$ ahead, with a longitudinal Root-Mean-Square (RMS) error of $1.8m$ and a lateral RMS error of

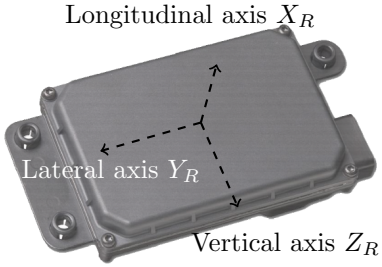

Figure 1: Delphi ESR radar, with associated frame used in this paper, adapted from [Del, 2013].

$0.4m$. At a unit price of around 2500 $US, with potential for a reduced price when purchasing large quantities, the authors concluded that the Delphi ESR was the best sensor of all three in term of performance-cost ratio, for detecting cars in this application. In [Wang *et al.*, 2011] the authors combined the Delphi ESR with a monocular vision camera for on-road obstacle detection using a novel three-level fusion approach based on visual attention, point alignment, region searching, and adaptive thresholding algorithm. This work was centered on the detection of cars, motorcycles and pedestrians. Other aspects of the performance of this radar need to be considered for robotic applications, such as the ability to detect other types of targets (e.g. trees, poles, fences), the performance with static vs. dynamic targets, the influence of clutter, sensor temperature, or material nature. A performance analysis for robotics should also concentrate on the sensor's performance at shorter ranges.

Prior work in the area of range sensors characterisation for robotics applications includes [Ye and Borenstein, 2002]. This well-known paper proposed a characterisation of the SICK LMS200 laser scanner, which has proved to be a very popular sensor in robotics. The work evaluated the general accuracy of measurements and identified elements that have an influence on the sensor's performance such as drift effect over time, target surface properties, and target distance. More recently, [Kneip *et al.*, 2009] used a similar strategy to characterise the Hokuyo URG-04LX laser range finder. Radar

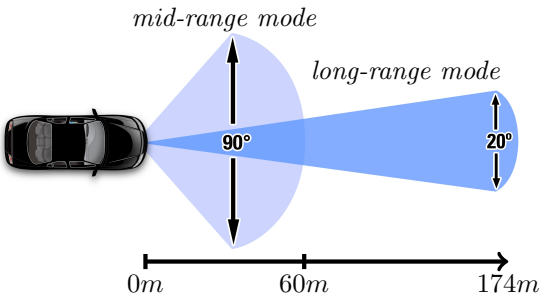

Figure 2: Radar detection zone from [Del, 2011]

characterisation papers are less common in the robotics literature. [Ryde and Hillier, 2009] proposed an extensive evaluation of the performance of a high-performance mm-wave radar designed by Brooker [Brooker, 2009] in the presence of airborne dust, in comparison with a SICK laser scanner and an optical sensor. However, this radar remains an order of magnitude more expensive than the Delphi ESR.

The procedure used in this paper is inspired from the characterisation strategies used in [Ye and Borenstein, 2002] and [Kneip *et al.*, 2009], however, it is adapted to the particularities of the Delphi radar. We first evaluate the accuracy of the detected target's position under varying sensor temperature and long time periods. We then consider the impact on the sensor's performance of different target's positions, speeds, shape and material, as well as clutter in the environment. Material penetration capability is also briefly considered.

2 The Delphi Electronically Scanning Radar

The Delphi Electronically Scanning Radar (ESR) has been designed to be used in the automotive industry for affordable forward detection systems on cars. As opposed to classic radar systems that use multiple beams with mechanical scanning or several fixed, overlapping beams to perform measurements, this radar uses solid state technology with Simultaneous Transmit and Receive Pulse Doppler (STAR PD) Waveform to electronically perform forward detection, allowing functionality such as adaptive cruise control, forward collision warning, brake support and headway alert [Del, 2011]. The sensor comes as a compact packaging of dimensions $173.7 \times 90.2 \times 49.2mm$ and weights $575g$.

According to the data-sheet provided by Delphi [Del, 2011], the radar operates in two different detection modes simultaneously. As illustrated in Fig. 2, the *long-range* mode should be able to detect targets as far as $174m$, within a field of view of $\pm 10°$, whereas the *mid-range* mode would detect targets at a distance of up to $60m$, within a field of view of $\pm 45°$. The range and bearing measurements accuracy of the radar are given as a minimum of $\pm 0.25m$ and $\pm 0.5°$, respectively. A maximum of 64 targets can be tracked simultaneously by the Delphi ESR. The technical specifications given by the manufacturer are shown in Table 1.

Table 2: Radar data used in experiments

Data	Unit	Resolution
Range	m	0.1
Bearing Angle	deg. (°)	0.1
Power	dB	1
Internal Temperature	°C	1

The detection process of the radar is very high level. For each target detected, the sensor provides information on the estimated *centroid* of the detected object. This includes: the range to the centroid (which will be denoted r_R), its bearing angle (θ_R), its longitudinal and lateral speeds, its acceleration, and the power of the returned signal (Φ). Note that the sensor does not provide any direct measurement of the size of the target.

The data are transmitted from the radar to a computer using a CAN communication protocol at a nominal bus speed of $500kbps$, and the measurement rate is $20Hz$.

3 Methodology

In this paper, we evaluate and analyse the performance of the sensor in conditions typically found in mobile robotic applications. Firstly, we evaluate the ability of the radar to reliably detect a target depending on its position, its type and its proximity to another target (target separation). Secondly, for detected targets, we evaluate the range and bearing measurements accuracy under the influence of environmental elements such as (sensor) temperature and time, and for varying relative positions, speeds, nature and size of the target.

All experiments were performed in an open field area to limit the reflections from the environment. The detection zone evaluated was between $1m$ and $25m$ range. $1m$ corresponds to the minimum range in the radar specifications, and $25m$ was considered to be a sufficient maximum range for most current robotics applications. The window of bearing angles considered was between $-40°$ and $+40°$, since target detection was found to be unreliable at the $\pm 45°$ limits stated in Delphi's specifications.

Table 2 specifies the radar data elements that were used for the experiments in this paper. Note that the resolution of the range and bearing values are only $0.1m$ and $0.1°$, respectively.

Unless specified otherwise, in the experiments of this paper we used a laser range scanner (SICK LMS200) to provide reference measurements for range (r_L) and bearing (θ_L) (i.e. ground truth). It was configured at a $0.5°$ angle resolution with a range accuracy of $1cm \pm 4cm$, which is much lower than what is expected from a low-cost radar. Configured as such, the laser provides ac-

Table 1: Delphi ESR technical specifications, from [Del, 2013].

Parameter	ESR Long-Range Requirement	ESR Mid-Range Requirement
Minimum Range	< 1m (> 10dB target) < 1m (> 0dB target)	< 1m (> 10dB target) < 1m (> 0dB target)
Maximum Range	> 175m (> 10dB target) > 100m (> 0dB target)	> 60m (> 10dB target) > 50m (> 0dB target)
Range Accuracy	< +/-0.5m noise component with +/- 5% bias component	< +/-0.25m noise component with +/- 5% bias component
Range Discrimination for two targets at same angle & range rate	< 2.5m	< 1.25m
Minimum Range Rate	< -100m/s	
Maximum Range Rate	> +40m/s	
Range Rate Accuracy	< +/- 0.12m/s	
Range Rate Discrimination for two targets at same range & angle	< 0.5 m/s	
Acceleration	Acceleration to be generated as an output of the Tracker	
Minimum Lateral Relative Velocity	< -20 m/s	
Maximum Lateral Relative Velocity	> +20m/s	
Lateral Relative Velocity Accuracy	Lateral velocity is derived in the tracker based on change in measured angle vs. time. Accuracy in m/sec is a function of range.	
Azimuth Field of View	> 20deg	> 90deg
Azimuth Angle Centroid Accuracy	< +/- 0.3deg (corner reflector targets) < +/- 0.5deg (other targets)	< +/- 1.0deg
Azimuth Angle Resolution of two targets at same range & range rate	< 3.5 deg	< 12 deg
Vertical Field of View	4.2deg – 4.75deg	
Minimum Amplitude	< -10dB	
Maximum Amplitude	> 40dB	
Minimum Update Interval	>= 20Hz	
Minimum Target Tracking	64 fused targets total	

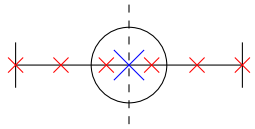

Figure 3: Top view of the reflector target as detected by the laser scanner (red crosses). The target's centroid position (large blue cross) given by the laser is calculated as the mean position of the red crosses.

curate range measurements for bearing angles varying from $\theta_L = -90°$ to $\theta_L = 90°$ with increments of 0.5°. In the experiments of this paper, for most targets the laser actually returns multiple points corresponding to the detected surface, while the radar only provides the measured position of one *centroid* for each detected target. Therefore, to obtain a reference position for the centroid of each target, we only used targets whose front face (as seen by the laser) was relatively flat, and the reference centroid position was computed as the mean of the range and bearing of the laser points on the surface of the object (the red crosses in Fig. 3). The data from the laser scanner is sent to the PC over a serial communication at a baud rate of 38.4 kbps.

4 Experimental Setup

Fig. 4 shows the experimental setup that was used for the different characterisation experiments. The radar was fixed on a support centered at $65cm$ above the ground (the Delphi manual specifies that the radar should be between $30cm$ and $86cm$ above the ground when mounted

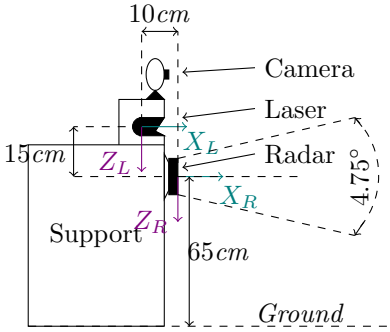

(a) Sensor configuration

(b) Reflector

Figure 4: Experimental setup. (a) Configuration of the sensors (side view). (b) Radar reflector used as standard target in some of the experiments.

on the front of a car). The SICK LMS200 laser scanner, providing the reference measurements, was placed on the support above the radar, along with a camera to visually monitor the experiments post-acquisition. We defined two right-handed coordinate sensor frames: 1) (X_R, Y_R, Z_R) centered on the radar, whose origin is at the radar's ($r_R = 0, \theta_R = 0$) detection point, and 2) (X_L, Y_L, Z_L), centered on the laser, whose origin is at the laser's ($r_L = 0, \theta_L = 0$), as illustrated in Figs. 4a and 5. In this setup, the two vertical axes (Z_R and Z_L) were parallel, both perpendicular to the ground.

In this configuration, the laser's measurement plane was $15cm$ above the radar's (vertical offset). To be

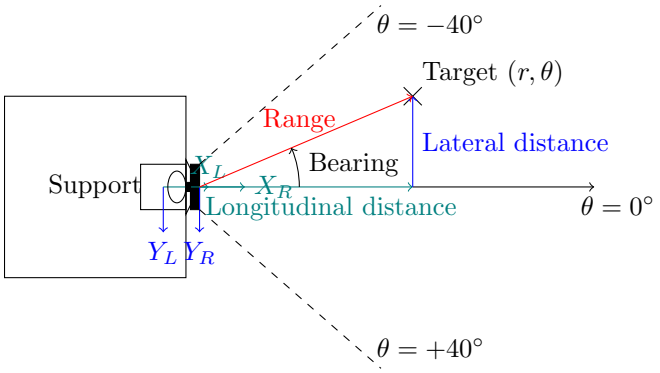

Figure 5: Radar frame and conventions (top view).

able to systematically use the laser as a reference, all targets considered in this paper were placed such that their front face was perpendicular to the ground, ensuring consistent range measurements between the two sensors. The origin of the laser frame was positioned with a longitudinal offset of $-10cm$ from the radar's origin to avoid any influence of the body of the LIDAR on the radar's perception. This longitudinal offset was systematically accounted for when processing the laser data, by transforming all measured points into the radar frame. However, the laser origin was at 0 on the radar's lateral axis, which means the coordinates of the origin of the laser frame in the radar frame were: $(x_R = -0.1, y_R = 0, z_R = -0.15)$.

Considering the resolution ($0.1m$ in range) and expected accuracy of the radar, measuring these translations with a standard ruler or measurement tape was considered sufficient for the experiments in this paper. However, the rotational alignment of the X and Y axes of the radar and laser frames (i.e. the azimuth alignment) was more critical, considering the impact such misalignment can have at large distances. The following simple calibration procedure was performed:

1. A small cylindrical radar reflector of diameter $0.1m$ (Fig. 4b) was placed at $(r_R = 25m, \theta_R = 0°)$ in the radar frame, i.e. along the longitudinal axis (X_R) of the radar. (Recall that $25m$ is the maximum range considered in this paper).
2. The laser was then rotated around its vertical axis (Z_L) until the reflector was measured at $\theta_L = 0$, aligning both sensor frames. Note that at $25m$ the laser returns only one point from the reflector. The reflector's diameter being $0.1m$, the maximum bearing error between the measured laser bearing and the actual position of the reflector's centre would be $0.11°$, which is much smaller than the expected angular accuracy of the radar.

The reference target used for this calibration procedure as well as multiple experiments in the following section was a $5cm$ radius, $40cm$-tall cylinder-shaped radar reflector shown in Fig. 4b. A $20cm$-high, $25cm$-wide and $2mm$-thick flat piece of cardboard was mounted on top of the reflector so that the laser scanner would detect points on a straight line passing through the center of the reflector. The position of the cardboard on the reflector was such that the laser beams could hit the cardboard while the radar beams would hit the reflector below without being affected by the cardboard (note that the radar sees through this thin cardboard). This setup allowed for precise positioning and constant orientation of the reflector during the experiments, and facilitated the calculation of the reference target's centroid position from the raw laser scans. The reference range and bearing for the centroid (i.e. the center of the corner reflector) were respectively computed as the mean values of the range and bearing of the laser points that hit the cardboard in a straight line (see Fig. 3). This could then be compared to the positions measured by the radar. Using the laser configured in $1cm$ and $0.5°$ resolution, the center of the reflector could then be measured with an accuracy of $\pm 4cm$ in range and $\pm 0.25°$ in bearing (for comparison, this corresponds to a width of about $\pm 10cm$ at $25m$ range). A similar operation was performed to compute the reference position of the other targets used in other experiments.

In the paper, the measurement accuracy is quantified using the mean value of a set of N measurements x_i:

$$\bar{x} = \frac{1}{N} \sum_{i=1}^{N} x_i \tag{1}$$

and the standard deviation:

$$\sigma(x) = \sqrt{\frac{1}{N} \sum_{i=1}^{N} (x_i - \bar{x})^2}. \tag{2}$$

The absolute error for a measurement x_R will be denoted $\epsilon(x)$ and given by: $\epsilon(x) = x_R - x_L$, where x_L corresponds to the reference measurement from the laser scanner (after offset compensation). For static targets, unless specified otherwise 500 data points were collected to compute the mean values of position measurements.

The experimental radar data were gathered using a custom Robotic Operating System (ROS) driver to interface the CAN communication. Processing and visualisation of both sensor was done using the `sicktoolbox_wrapper` and `Rviz` ROS packages.

Experiments were performed outdoors in a open field area, with an ambient temperature of $22 \pm 5°C$. Any deviations from these nominal experimental conditions are indicated in the paper where appropriate. Note that most experiments were conducted in clear environmental conditions, i.e. without presence of airborne dust, smoke, or rain, so that the laser scanner could be used as a reliable reference. The ability of a mm-wave

radar beams to see through this type of environmental phenomena is considered well known from the literature [Brooker, 2009], therefore it is not addressed in the experiments of this paper, with the exception of vegetation in Sec. 5.8.

5 Characterisation experiments

In this section we characterise the sensor's performance for obstacle detection in field robotics. We first evaluate the accuracy of the detected target's position under varying sensor temperature and long time periods. Then we consider the impact on the performance of different target's positions, speeds, shape and material, as well as clutter in the environment. We also consider material penetration capability.

5.1 Sensor temperature

To observe the potential impact of the internal temperature of the sensor on measurements, the standard reflector was placed at $(r = 15m, \theta = 0°)$ in the radar frame and samples were recorded from the initialisation of the sensor until temperature stabilisation. A built-in thermometer communicated the sensor temperature in real time using the CAN bus. Fig. 6 depicts the evolution of the radar measurements' absolute errors in range, bearing as well as the evolution of the signal power over time as the internal sensor temperature increases. The sensor temperature started at $25°C$ when the sensor was powered on and eventually stabilised at $40°C$. During that period, the average range error was around $15cm$ with oscillations between $+50cm$ and $-40cm$, the average bearing error was around $0°$ with oscillations between $+1°$ and $-1°$, and the signal power fluctuated frequently between $0dB$ and $-10dB$. The behaviour of the different measurements does not appear to be directly related to the change of temperature, as the perturbations observed occur at a much smaller time scale than temperature changes.

5.2 Time period

To test whether a drift effect could be observed when measuring a target's position over long periods of time we placed the standard reflector at $(r = 15m, \theta = 0°)$ in the radar frame and recorded radar measurements every $50ms$ $(20Hz)$ for a total of 1h15min (90000 measurements) in an open field with fixed experiment conditions and stabilised sensor temperature. Short-term perturbations possibly linked to random outdoor environment effects such as gusts of wind can be observed over time, however, no clear drift of the measurements could be observed in the data (not shown due to space limitations).

5.3 Relative position of the target

To appraise the influence of the position of the target on the radar's target detection capabilities and measurements accuracy, the standard reflector was placed at

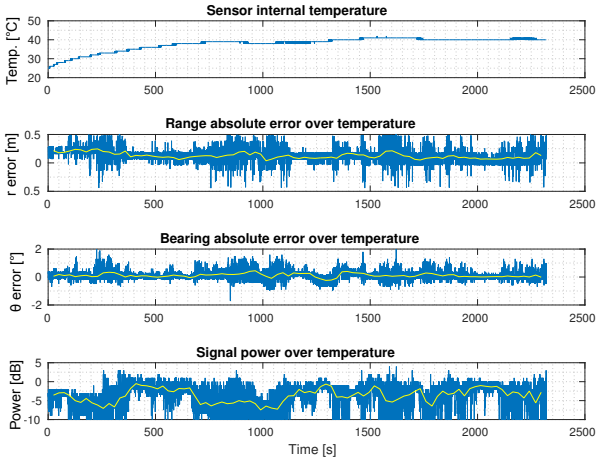

Figure 6: From top to botton, evolution in time of: sensor temperature, absolute error in range, absolute error in bearing, and signal power.

ranges between $1m$ and $25m$ by steps of $1m$ and bearing angles of $-40°, -20°, 0°, +20°, +40°$. For each of these positions, the radar was static during the collection of 500 data points, used to compute a mean value of the range and bearing measurements.

Fig. 7 shows the mean detected positions in polar coordinates. In term of target detection ability, the radar was able to detect the target at much longer ranges when the bearing angle was close to zero degree, which could be related to the long-range and mid-range detection zones used by the radar. The minimum distance for which the target was detected was within $r = 2m$ and $r = 3m$, and the maximum detection distance varied between only $r = 9m$ for $\theta_L = -40°$, and $r = 25m$ for $\theta_L = 0°$. This result is significantly different from the technical specifications given by Delphi, which announced a minimum range detection of $1m$ for both mid-range and long-range modes and a maximum detection range greater than $50m$ for the mid-range window.

Fig. 8 shows the mean range and bearing absolute errors for all the positions of the reflector where it was actually detected reliably. The standard deviation of the measurements at each position are also shown as vertical bars of the same color as the data points.

The range *absolute* error can be seen to generally decrease as the target's distance increases, starting with a positive error and ending with a negative value. This behaviour appears to be similar for the various bearing angles. For instance, at $\theta = 0°$ the range absolute error is $0.1m$ at the first detection $2m$ away from the radar, and gradually and slowly decreases to reach $-0.45m$ for the last recorded data point at $r = 25m$. This result is comparable to the $\pm 0.5m$ range accuracy announced by the manufacturer in the technical specifications of the radar (see Table 1).

The bearing angle *absolute* error $\epsilon(\theta)$ appears to be-

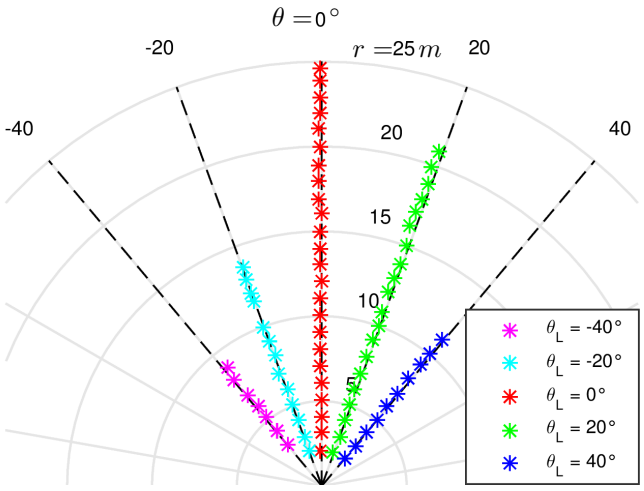

Figure 7: Detections and corresponding position measurements made by the radar, shown in polar coordinates. θ_L indicates the reference bearing angles given by the laser.

come smaller as the range is increasing. This result is most likely due to the target becoming smaller as it is moved away from the sensor, which means the centroid of the target became more likely to be computed in the center of the target, which is translated into a smaller bearing error. The bearing angle value also seems to impact the behaviour of the bearing error, which tends to have a mean value more positive for negative bearing angles, and a mean value more negative for positive bearing angles. This error behaviour can be observed in Fig. 7: the target is detected closer to the sensor than it actually is. Note that the radar is very accurate for targets on the longitudinal axis: the mean value of the bearing absolute error at $\theta_L = 0°$ is $\epsilon(\theta) = -0.4°$ which is close to the resolution obtained with the laser scanner.

The bearing accuracy results obtained here are comparable to the technical specifications of the radar with $\pm 0.4°$ in the $\pm 10°$ window and $\pm 1°$ in the $\pm 45°$ window.

The standard deviation of the errors, shown as the vertical bars of the same color of the data points in Fig. 8, are consistently very small and did not appear to be affected by the position of the target. The average standard deviation was $\sigma(r) = 6cm$ over all measured range values and $\sigma(\theta) = 0.1°$ over all measured bearing angles.

The position of the target did not appear to have a clear impact on the power measurements, which were repeatedly varying between $0dB$ and $-10dB$.

5.4 Relative speed of the target

In mobile robotics applications, most obstacles would be moving in relation to the sensor. In order to evaluate how the target's speed direction and amplitude influences the radar measurements accuracy, two experiments were performed.

The first experiment used a human as a dynamic tar-

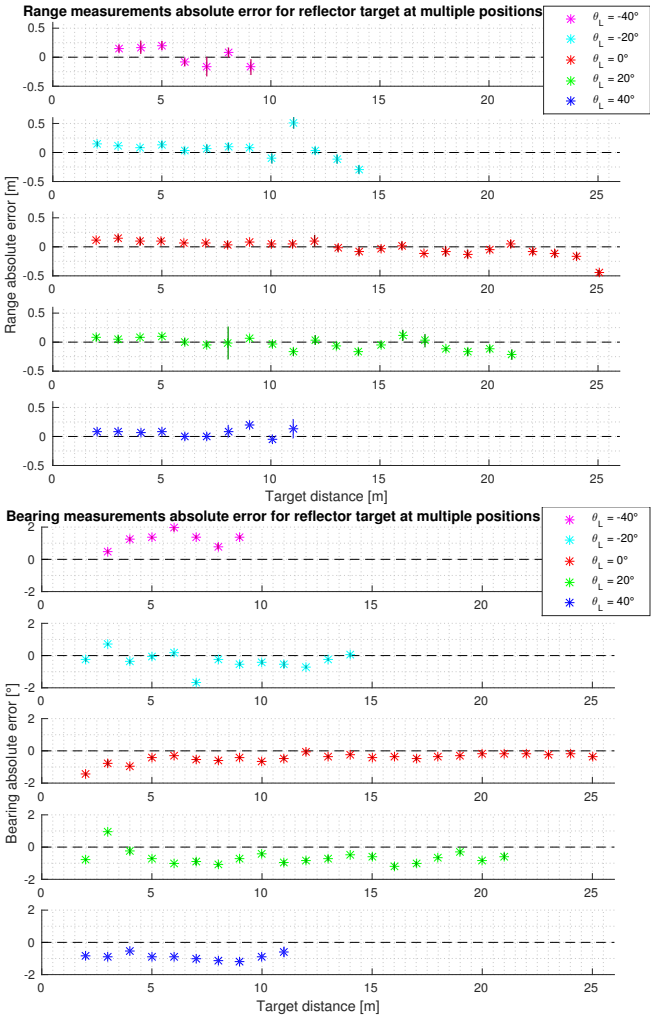

Figure 8: Range and bearing average absolute error for multiple positions

get, moving radially (i.e. with constant bearing angle) at a constant speed, from $r = 1m$ to $r = 25m$. Different speed amplitudes were tested for bearing angles of $-40°, -20°, 0°, +20°, +40°$.

Fig. 9a depicts the result of a linear interpolation of the data points from the evolution of the range measurement errors (a) and bearing measurement errors (b), for each radial speed considered. These lines were computed using the Matlab "polyfit" function to produce a linear least-squares line from the scattered points.

The radial speed had a clear impact on the range measurement accuracy, however, it did not seem to impact the bearing measurement accuracy (therefore, due to space limitation, the latter is not shown in the paper). A positive error in range can be observed in the case of positive speeds while a negative error can be seen for the negative speeds. In all cases the magnitude of this error increases as the magnitude of the speed increases. For all speeds there is a relatively consistent decrease of the

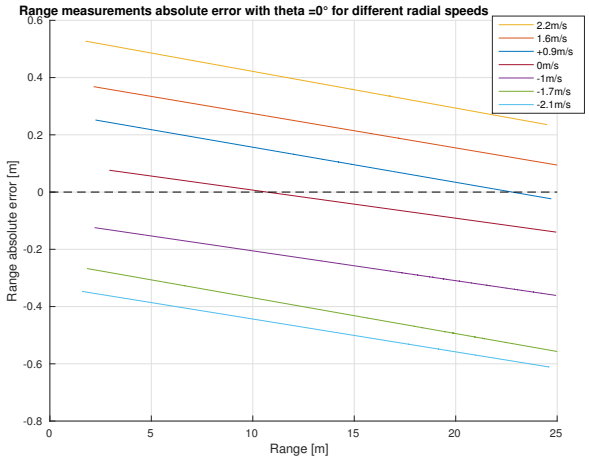

(a) Range error for different radial speeds

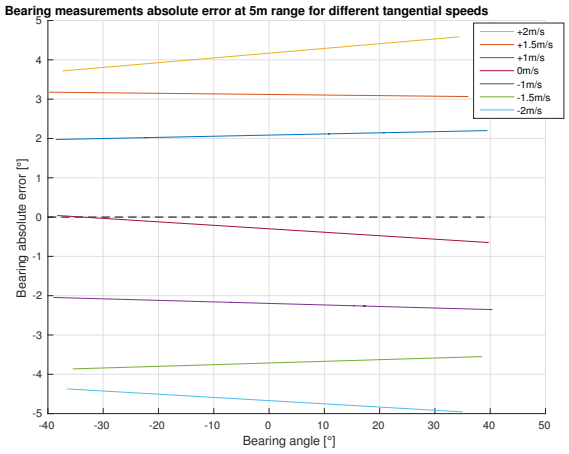

(b) Bearing error for different tangential speeds

Figure 9: Influence of target speed on range (a) and bearing (b) error.

absolute range error as the range increases (i.e. the target seems to appear closer to the radar than it really is). The range accuracies obtained in this experiment were mostly within the bounds given in the specifications of the radar, however, we expect at higher velocities (e.g. for dynamic targets faster than a pedestrian), the performance would degrade further.

The second experiment used a human moving in a tangential direction for fixed ranges of $5m$ and $10m$, respectively. Fig. 9b shows the bearing angle absolute error with respect to the reference bearing angle, for different tangential speeds using the same curve fitting process as in the previous experiment. A positive error can be seen for all positive speeds while a negative error was obtained for all negative speed. The magnitude of this error is seen to increase with the magnitude of the speed. This means that in general the target was detected ahead of its real position. The bearing accuracies obtained in these tests were lower than those in the technical specifications with up to $\pm 4°$ of error. It is possible that

Table 3: Influence of tree trunk width on bearing accuracy for $r = 15m$.

Target Width [m]	$\epsilon(\theta) \pm \sigma(\theta)$ [°]	Lateral error [m]
1.3	-2.94 ± 0.96	-0.770 ± 0.251
0.7	-0.14 ± 0.26	-0.037 ± 0.068
0.15	0.03 ± 0.13	0.008 ± 0.034
0.1	-0.02 ± 0.06	-0.005 ± 0.016

the manufacturer's accuracy values were obtained for a static target.

Note that the target's relative speed did not have any particular observable effect on the power measurements.

5.5 Size of the target

The size of the target is likely to have a significant impact on the radar's measurements, for two main reasons: 1) for any radar the power of the signal returned tends to increase with the size of a target, although it is difficult to separate this from the influence of the material the target is made of and the shape of its surface; 2) this particular radar returns the centroid of the target, whose accuracy is expected to vary with the width of the object.

An experiment was set up using tree trunks of different diameters placed at the same position of ($r = 15m, \theta = 0°$) to compare the measurements obtained. Table 3 shows the mean absolute errors in bearing obtained as well as the associated standard deviations.

It can be seen that the size of the tree trunk had a direct effect on the bearing error mean and its standard deviation: both are seen to increase as the size of the target increased. For the tree trunk of $1.30m$ width, the error was notably larger, as the centroid of the target was actually positioned at the left edge of the trunk. The last column of Table 3 shows the corresponding lateral error on the position of the centroid. It can be seen that most measurements still place the centroid somewhere on the surface of the trunk.

5.6 Nature of the target

In this experiment, a few common objects that can be encountered on a field robotics application were placed in the detection zone of the radar at $\theta = 0°$ and $r = 5, 10, 15, 20, 25m$. They were all static during the measurements. The range, bearing and power measurements were recorded to compare the radar's performance with the different targets, and at each position the mean error over 500 measurements was computed, similarly to prior experiments. The objects considered were: the standard reflector, a $1.8m$-tall human, a $70cm$ diameter tree trunk, and a $20cm$ diameter metal pole. Fig. 10 shows the different targets, and Table 4 shows the range and bearing absolute errors and standard deviations for the different range values. It also shows in what interval the power values were seen to vary for each target.

Table 4: Signal power boundaries, and Range and Bearing average absolute error and standard deviation for different obstacles at $r = 5, 10, 15, 20, 25m$ and $\theta = 0°$

		Range [m]				
Obstacle	$[min(\Phi), max(\Phi)][dB]$	5	10	15	20	25
Reflector	[-10;6]	$0.10 \pm 0.03m$ $-0.42 \pm 0.09°$	$0.05 \pm 0.04m$ $-0.64 \pm 0.06°$	$-0.03 \pm 0.04m$ $-0.4 \pm 0.01°$	$-0.05 \pm 0.03m$ $-0.33 \pm 0.10°$	$-0.15 \pm 0.04m$ $-0.26 \pm 0.13°$
Human	[-10;-3]	$0.11 \pm 0.07m$ $0.00 \pm 1.3°$	$0.11 \pm 0.07m$ $0.12 \pm 0.71°$	$-0.03 \pm 0.22m$ $0.22 \pm 0.37°$	$0.09 \pm 0.15m$ $0.22 \pm 0.29°$	$-0.04 \pm 0.17m$ $0.28 \pm 0.36°$
Tree	[-10;-8]	$0.10 \pm 0.13m$ $1.21 \pm 0.94°$	$0.07 \pm 0.06m$ $0.35 \pm 0.13°$	$0.24 \pm 0.06m$ $-0.63 \pm 0.17°$	$-0.64 \pm 0.17m$ $0.40 \pm 1.02°$	$0.19 \pm 0.16m$ $-0.18 \pm 0.64°$
Metal Pole	[-4;4]	$0.12 \pm 0.00m$ $-0.65 \pm 0.00°$	$0.14 \pm 0.05m$ $-0.56 \pm 0.05°$	$0.19 \pm 0.05m$ $-0.19 \pm 0.03°$	$0.07 \pm 0.03m$ $-0.32 \pm 0.22°$	$-0.07 \pm 0.07m$ $-0.48 \pm 0.54°$

(a) Human

(b) Tree Trunk

(c) Metal pole

Figure 10: Targets used in experiment

The range measurements accuracy varies between the different types of target, with error values generally close to $0.1m$, except for the tree trunk which was sometimes detected with up to $0.6m$ range error. At short range the standard deviation of the range measurements appears to be significantly smaller for the reflector and the metal pole target than the human and the tree, which is probably related to the metallic surfaces. However, that difference attenuates at longer range.

The bearing angle accuracy is generally under 0.5° which is close to the accuracy of the centroid position obtained from the laser scanner. A notable exception is the tree at $5m$ with an angular error of more than 1°.

Fig. 4 also shows in what interval the power values were seen to vary for each target. The power measurements behaviour changes broadly from one type of target to another. Fig. 11 depicts examples of power measurements data for two of the targets: the reflector and the human. For the former, the power values change widely between two positions, but the standard deviation for each position is fairly small (under $1dB$). For the latter (the human), the values are quite consistent between two successive positions, but the standard deviation is much larger, with an average of $3dB$ and a maximum of $4dB$.

Detecting humans is often particularly important in robotics applications. Fig. 12 shows the range and bearing measurements obtained for the human target. The position of the human was detected with an average range error of $0.04 \pm 0.1m$ and bearing error of $0.1 \pm 0.6°$,

Table 5: Target detection for two human targets

Range [m]	Separation Frontier [m]	Separation Angle [°]
15	2.5	9.5
10	1.5	8.5
5	1	11.3

which is relatively close to the range accuracy and angular resolution of the laser scanner.

5.7 Clutter in the environment

To evaluate the ability of the radar to separate targets, a static human target was placed at $r = 5, 10, 15m$ and $\theta = 0°$, and a second human target was then placed $4m$ away from the first human perpendicularly to the longitudinal axis. The latter then very slowly moved closer to the first target by following a straight line, while measuring all the positions with the radar and the laser scanner. This procedure is illustrated in Fig. 13a.

Table 5 shows the distance at which the detection of the target passed from reliably detecting two separated targets, to one detected target at a position between the two real targets, i.e. the "Separation Frontier". The separation frontier appears to consistently decrease as the range decreases. It corresponds to an angle of separation of about 10°, which is consistent with the technical specifications.

5.8 Material penetration

Radar waves have the advantage to be able to penetrate through some material depending on their frequency [Matthies *et al.*, 2005]. With a frequency of $76.5GHz$, it can be expected that the Delphi ESR waves would be able to penetrate through some thin material before detecting a target. For example, we observed that the sensor can reliably detect targets behind thin cardboard or posters.

In this experiment we evaluated the effect of foliage layers placed between the standard reflector and the radar. The standard reflector was placed at $r = 5, 10, 15m$ and $\theta = 0°$, and successive foliage layers were added at $1m$ range ahead of the reflector. The type of

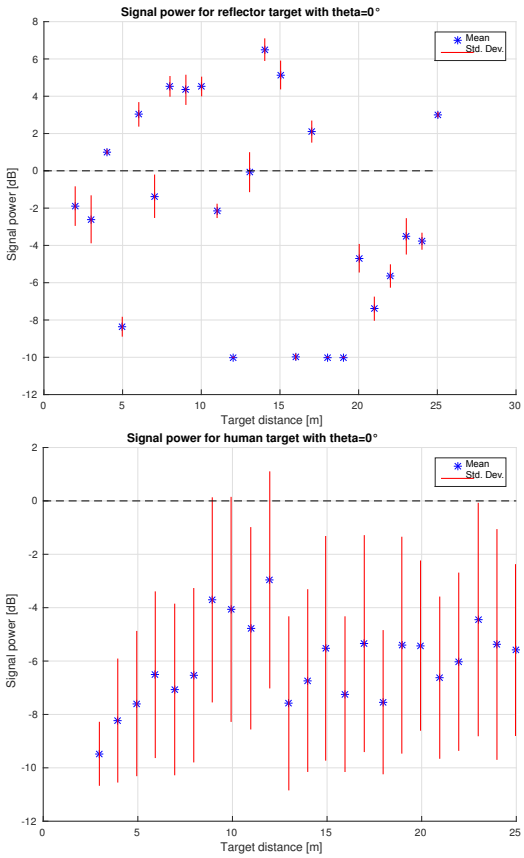

Figure 11: Power measurements for the standard reflector (top) and a human target (bottom) at $\theta = 0°$.

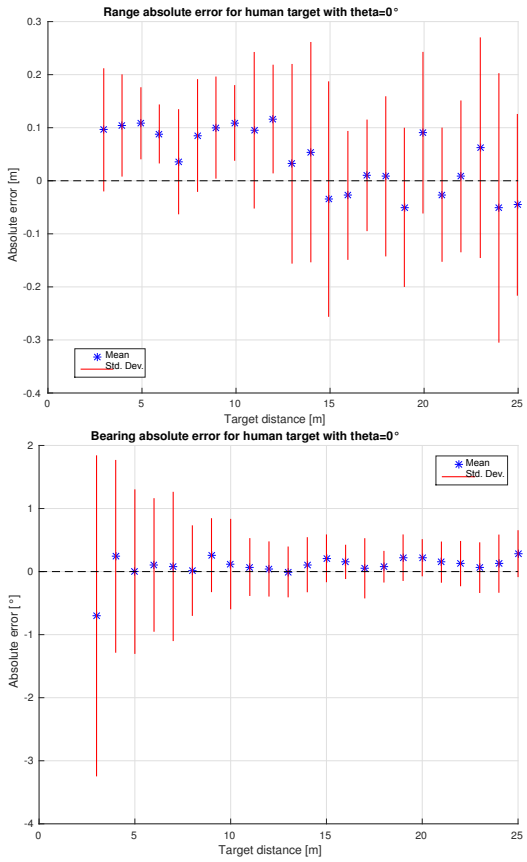

Figure 12: Range (top) and Bearing (bottom) absolute errors for a human target at $\theta = 0°$ bearing.

foliage used for the experiment is shown in Fig. 13b, each layer covered partially the view and was a few mm thick.

Table 6 shows the rate of detection of the standard reflector at different ranges and for different layers of foliage. The detection percentage is calculated from the number of samples for which the target or foliage is detected, out of the 500 samples recorded at each position. As expected, the detection rate of the target and the power both decrease as more layers are added in front of the reflector, while naturally the detection rate of the foliage increases. The range separating the target from the radar also played a role in penetration capability, as the target's detection rate is higher for a higher number of layers at closer range.

6 Conclusion

This paper presented an experimental characterisation of the Delphi Electronically Scanning Radar (ESR) for mobile robotics applications. Radars have an important role to play in field robotics for applications that require reliable perception in all-weather conditions or in dusty environments such as for mining. The Delphi ESR has been designed primarily for use in automotive applications to detect obstacles such as cars, pedestrians and bicycles at long distances, however, its performance at shorter ranges, more typically useful in current mobile robotics, is largely unknown. In this paper we focused on ranges inferior to $25m$.

We evaluated target detection abilities of the radar, as well as the accuracy on the measured positions of detected targets by comparing with a SICK laser scanner in conditions that generally do not affect the latter. The targets considered included a cylindrical reflector, humans, tree trunks and poles. The following summarises the main findings of analysis in this paper, in particular those that seem to differ significantly from the technical

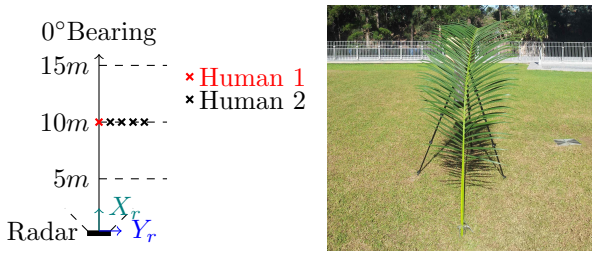

(a) (b)

Figure 13: (a) Experiment setup for target separability evaluation. (b) Two layers of foliage used in front of the target.

Table 6: Standard reflector detection rates through foliage

Range [m]	Vegetation Layers	Power of Target [dB]	Target Detection	Foliage Detection
5	0	10 ± 0	100%	0%
	1	2 ± 2	100%	0%
	2	-4 ± 3	100%	3%
	3	-10 ± 0	0%	100%
10	0	2 ± 1	100%	0%
	1	-6 ± 4	95%	10%
	2	-7 ± 3	90%	10%
	3	-10 ± 0	2%	98%
15	0	-7 ± 3	100%	0%
	1	-9 ± 1	50%	50%
	2	-10 ± 0	50%	50%
	3	-10 ± 0	10%	80%

specifications given by the manufacturer.

The results in this paper indicate that the performance of the ESR is not significantly affected by the sensor's temperature, and no clear drift of the measurements was observed over a long time period. The target detection ability was strongly affected by the azimuth of the target, with short maximum detection range on the sides (as low as $9m$ at $-40°$ bearing), compared to the center (bearing angle $\theta = 0$) where targets were detected reliably at all distances considered from about $2m$. The range accuracy was found to worsen as the target's radial speed was increasing (e.g. $0.5m$ error at $2.2m/s$ vs. about $0.25m$ for static targets) with the sign of the error corresponding to the sign of the speed. The bearing accuracy was also affected by the target's tangential speed (up to $5°$ error at $2m/s$).

The bearing accuracy was affected by the size of the target, especially, an effect that seems to increase with the size of the target, probably due to the fact that the radar only provides a measure of the centroid of the target. However, the influence of the nature of the target on the position accuracy did not seem to be strong.

The target separation limit was found to be around $10°$ bearing angle. The radar was shown to be able to detect targets behind thin layers of vegetation, including when these targets were hardly visible to the human eye, or to a laser scanner.

Although Delphi suggests the use of the power of the signal to distinguish between different types of targets (e.g. between a human and a car), this does not seem to be viable due to the large variances of power observed in this paper for different positions of the same target (e.g. the reflector used in this study), and in some cases for a fixed position (e.g. when detecting a human).

Overall, the Delphi ESR offers strong performances with a range accuracy within $0.25m$ and a bearing accuracy within $1°$ in most cases. The performance is especially good when targets are mostly right in front of the sensor ($\pm 10°$ azimuth). However, its limited ability to detect target placed more on the sides is a concern. Even though the sensor can theoretically track up to 64 targets at the same time, a major limitation is the fact that only the position of the centroid of each target is provided, with no indication of the size of the target.

Acknowledgments

This work was supported by the School of Electrical Engineering and Computer Science, at Queensland University of Technology, and by Polytech Paris-UPMC.

References

[Brooker, 2009] G. Brooker. *Sensors for Ranging and Imaging*. SciTech Publishing, Inc., 2009.

[Del, 2011] Delphi Automotive Systems. *Delphi ESR Datasheet*, 2011. Available at `http://delphi.com`.

[Del, 2013] Delphi Automotive Systems. *Delphi ESR Startup Guide*, 2013. Available at `http://www.delphi.com`.

[Fischer *et al.*, 2009] J. Fischer, A. Menon, A. Gorjestani, C. Shankwitz, and M. Donath. Range sensor evaluation for use in cooperative intersection collision avoidance systems. In *Vehicular Networking Conf.*, 2009.

[Gerardo-Castro and Peynot, 2012] M. P. Gerardo-Castro and T. Peynot. Laser-to-radar sensing redundancy for resilient perception in adverse environmental conditions. In *Australasian Conf. on Robotics and Automation*, 2012.

[Kneip *et al.*, 2009] L. Kneip, F. T Ache, G. Caprari, and R. Siegwart. Characterization of the compact Hokuyo URG-04LX 2D laser range scanner. In *Int. Conf. on Robotics and Automation*, 2009.

[Matthies *et al.*, 2005] L. Matthies, C. Bergh, A. Castano, J. Macedo, and R. Manduchi. Obstacle detection in foliage with ladar and radar. In *The Eleventh Int. Symposium on Robotics Research*. Springer, 2005.

[Peynot *et al.*, 2009] T. Peynot, J. Underwood, and S. Scheding. Towards reliable perception for unmanned ground vehicles in challenging conditions. In *Int. Conf. on Robotics and Intelligent Systems*, 2009.

[Ryde and Hillier, 2009] J. Ryde and N. Hillier. Performance of laser and radar ranging devices in adverse environmental conditions. *Journal of Field Robotics*, 26(9):712–727, 2009.

[Wang *et al.*, 2011] T. Wang, N. Zheng, J. Xin, and Z. Ma. Integrating millimeter wave radar with a monocular vision sensor for on-road obstacle detection applications. *Sensors*, 11(9), 2011.

[Ye and Borenstein, 2002] C. Ye and J. Borenstein. Characterization of a 2-D laser scanner for mobile robot obstacle negotiation. In *Int. Conf. on Robotics and Automation*, 2002.